Cell Reports
Physical Science

CellPress
OPEN ACCESS

Article

In situ monitoring of protein transfer into nanoscale channels

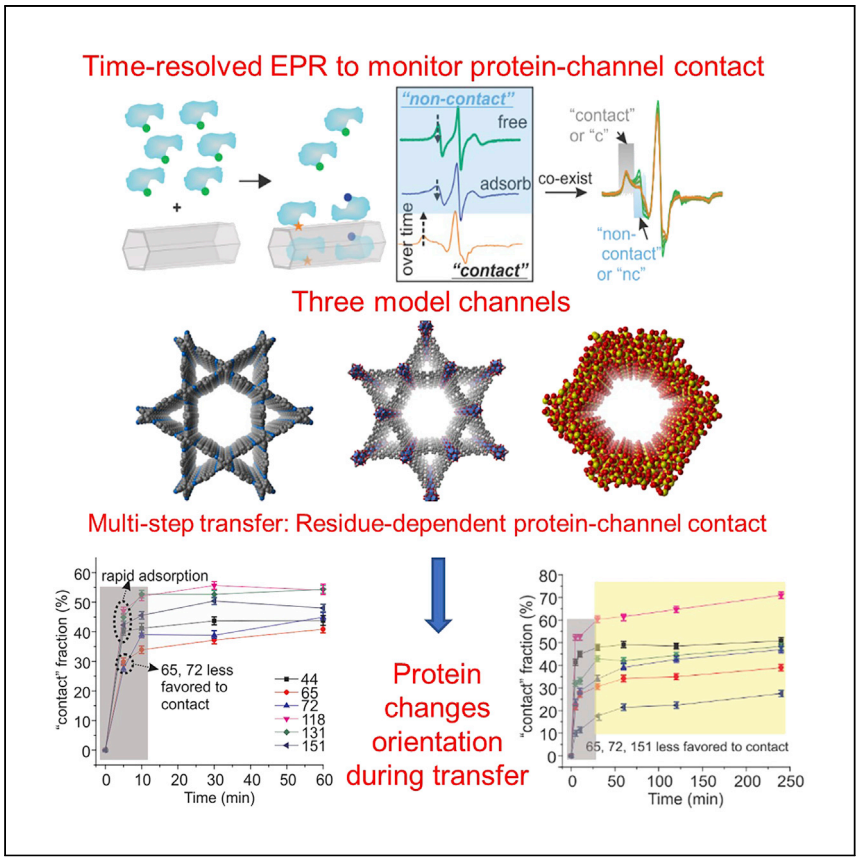

Pan et al. report the orientation changes of a model protein upon transfer into three nanoscale channels that differ in surface hydrophobicity (but a similar diameter). The findings may be useful for guiding the rational design of synthetic materials to host enzymes and/or mimic the cellular compartments.

Yanxiong Pan, Xiaoliang Wang, Hui Li, ..., Heedeok Hong, Zhongyu Yang, Shengqian Ma

zhongyu.yang@ndsu.edu (Z.Y.)
shengqian.ma@unt.edu (S.M.)

Highlights

Protein transfer into nanoscale channels differing in hydrophobicity is demonstrated

Multi-step protein transfer is observed for charged and hydrophobic channels

Protein changes its orientation depending on the channel surface properties

Time-resolved EPR spectroscopy can reveal residue-level details of protein transfer

Pan et al., Cell Reports Physical Science 2, 100576
September 22, 2021
https://doi.org/10.1016/j.xcrp.2021.100576

Cell Reports
Physical Science

CellPress
OPEN ACCESS

Article

In situ monitoring of protein transfer into nanoscale channels

Yanxiong Pan,[1,5] Xiaoliang Wang,[2,5] Hui Li,[1] Junyu Ren,[4] Yin Zhang,[4] Drew Jordahl,[1] Isabelle Schuster,[1] Jasmin Farmakes,[1] Heedeok Hong,[3] Zhongyu Yang,[1,*] and Shengqian Ma[4,6,*]

SUMMARY

Protein transfer into nanoscale compartments is critical for many cellular/life processes, yet there are few reports on how compartment properties impact the protein orientation during a transfer. Such a knowledge gap limits a deeper understanding of the protein transfer mechanism, which could be bridged using nanoporous materials. Here, we use a mesoporous silica, a covalent organic framework, and a metal-organic framework with charged, hydrophobic, and neutral surfaces, respectively, to elucidate the impact of channel properties on the transfer of a model protein, lysozyme. Using site-directed spin labeling and time-resolved electron paramagnetic resonance spectroscopy, we reveal that the transfer can be a multistep process depending on channel properties and depict the relative orientation changes of lysozyme upon transfer into each channel. To the best of our knowledge, this is the first structural insight into protein orientation upon transfer into different compartments, meaningful for the rational design of synthetic materials to host enzymes or mimic the cellular compartments.

INTRODUCTION

Protein transfer into artificial or cellular/native compartments with nanoscale dimensions is essential for both fundamental protein research[1–6] and several cellular processes.[7–12] In particular, loading enzymes into synthetic mesoporous materials is essential for enzyme confinement that improves biocatalysis[5] and understanding fundamental protein structure/dynamics under spatial confinement.[6,13,14] In cells, transferring proteins into chaperones is critical for protein folding and chaperone-assisted protein sorting/translocation.[15,16] Furthermore, protein transfer into "protein-conducting" channels[17–21] is the first step of protein translocation among cellular organelles[8–12,22–34] and is relevant to several genetic diseases or peroxisomal disorders.[35,36] Understanding the mechanism of protein transfer is therefore critical for guiding the rational design of compartments that minimize protein alteration during translocation or therapeutics targeting protein translocation failures.[37–42]

Although exciting, current progress on protein transfer research has been mainly focused on constructing novel mesoporous compartments,[43–45] revealing the driving force of protein transfer into compartments, and understanding the consequences of the transfer.[35,36,46,47] A fundamentally important aspect, changes in protein structure and relative orientation upon transfer into a compartment, is often missing, which prevents revealing the cause of potential protein alteration or damage during a transfer. Of particular importance is protein orientation because it depends on the contact between specific protein regions/residues and compartment;

[1]Department of Chemistry and Biochemistry, North Dakota State University, Fargo, ND 58102, USA

[2]Department of Chemistry, University of South Florida, Tampa, FL 33620, USA

[3]Department of Chemistry, Michigan State University, East Lansing, MI 48824, USA

[4]Department of Chemistry, University of North Texas, Denton, TX 76203, USA

[5]These authors contributed equally

[6]Lead contact

*Correspondence: zhongyu.yang@ndsu.edu (Z.Y.), shengqian.ma@unt.edu (S.M.)

https://doi.org/10.1016/j.xcrp.2021.100576

such interaction can initialize/assist in protein loading and induce the needed structural changes to facilitate the transfer. Protein orientation is also essential for their functionality/catalytic activity because protein activity is dependent on not only the amount of available proteins but also how efficiently a protein can recognize the correct substrate, bind to it, and re-orient to expose the active site so that efficient contact between the substrate and the active site is reached. For a protein immobilized on a solid material, protein orientation with respect to the surface of the channels is critical for substrate access to the active site. An improper orientation (i.e. those partially bury the active site) will directly lead to reduced catalytic activity.

Probing protein orientation changes during transfer requires knowledge on protein regions that contact the compartment in real time. Furthermore, due to the heterogeneity in native compartments,[48] it is more important to reveal how compartment properties influence protein orientation upon transfer into a compartment. Generally, the contact regions are dependent on protein-compartment interactions,[49–55] which may be predicted computationally. However, experimental validation is always required. Probing protein orientation upon transfer in cells is even formidable, if not impossible,[48,56–58] due to the difficulty in directing a protein to be transferred into a cellular compartment. *In vitro* reconstruction of cellular channels is also not ideal due to the lack of control in channel properties[59] and the difficulty in providing the complicated molecular interactions to form the channel. Although protein transfer to inorganic materials has been investigated,[1,2,60] monitoring protein orientation upon loading into these compartments is challenging due to the lack of proper protein-probing techniques that are immune of the compartment backgrounds. Furthermore, most of the artificial materials, including silica mesoporous materials and active carbon,[61] have heterogeneous pore sizes[13,62–66] and are thus not ideal for understanding the impact of channel properties on the transfer. Recent advances in metal-organic framework/covalent organic framework (MOF/COF) research offer an opportunity to construct artificial nanoscale channels with tunable and uniform geometry and hydrophobicity, making MOFs/COFs preferential platforms for probing protein transfer.[45,67–72] Also, many biological channels are often on the order of a few nanometers in diameter, close to the size of the MOF/COF channels.[17–19] However, the background signals of MOFs/COFs can still complicate data interpretation of most protein-probing approaches. Protein interaction in narrow spaces such as chaperone cavities can be probed by NMR;[73–76] however, the orientation changes of protein translocation into narrow spaces remain elusive. Site-directed spin labeling (SDSL) in combination with electron paramagnetic resonance (EPR) spectroscopy[77,78] has been proven effective in probing protein structural information in porous materials including MOFs/COFs,[49,61,79] regardless of the background interference. Furthermore, time-resolved EPR is available that is suitable for monitoring the transfer process.

In this contribution, the orientation changes of a model protein, T4 phage lysozyme (T4L), upon loading into a series of nanoscale channels are explored. T4L has been extensively studied using SDSL-EPR.[80,81] Six solvent-exposable T4L sites scanning through key regions of T4L are spin labeled, one at a time, in order to probe the contact region of T4L during the transfer. To probe the effects of channel surface on protein transfer (while leaving the impact of diameter as our ongoing work), three channels with a similar size but different surfaces were selected (Figure 1A): COF-ETTA-TPDA (ETTA: 4,4′,4′′,4′′′-(ethene-1,1,2,2-tetrayl)tetraaniline; TPDA: [1,1′:4′,1′′-terphenyl]-4,4′′-dicarbaldehyde (~4.5 nm; hydrophobic interaction with T4L),[82] Mobil Composition of Matter No. 41 (~4.5 nm; electrostatic interaction), and Porous Coordination Network 128 (~4.6 nm; near-neutral surface).[83,84] These channels have a diameter

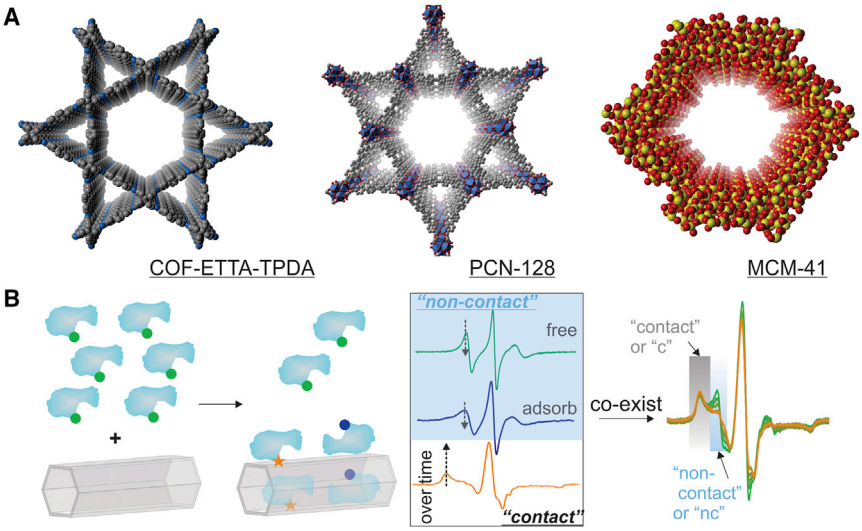

Figure 1. A summary of the experimental design of this work

(A) Schematic illustration of the structures of the three porous materials involved in this study.

(B) Principles of using time-resolved EPR spectroscopy to monitor protein loading and relative orientation in real time. The protein is labeled at a surface site (green dot); during a transfer, the labeled site can contact the channel (orange star) or hang out from the channel surface (blue dot). (Inset) The EPR signal of a spin label on a protein that is free in solution (green), upon adsorption to the surface of a channel (blue), and upon contact with a channel (orange) will result in different line shapes. During a transfer process, all three cases can co-exist, resulting a complex EPR spectrum with multiple spectral components. Over time, the non-contact component decreases (light blue shade), while the contact component increases (gray shade), indicating the transfer of protein into the channels.

that is slightly larger than T4L (2 × 3 × 4.5 nm), which allows the transfer to occur. The transfer of each labeled T4L mutant into each channel is monitored in real time, which reveals different loading steps among different materials (Figure 1B). Moreover, on the same channel, differences in the loading profile are observed among different labeled sites, suggesting preference in contact region, which reveals protein orientation at each step. Taken together, a molecular mechanism is proposed for T4L upon transfer into each channel. To our best knowledge, this is the first experimental report of the impact of confinement properties on the orientation changes of proteins upon transfer into nanoscale compartments. This knowledge serves as the structural basis of understanding how different cellular confinement properties select proteins and affect their transfer. This knowledge can also serve as the basic criteria of the effectiveness of developing artificial compartments to mimic the sophisticated cellular compartments, generating the excitement of using cell-free platforms to study the complicated cellular processes. Our results highlight the significance of using tunable, uniform, nanoscale synthetic materials to systematically investigate the interaction of artificial channels with biomolecules, elucidating the rational design of artificial compartments to mimic protein translocation processes in nature.

RESULTS

Synthesis and characterization of materials

MCM-41 and other chemical supplies were purchased from Sigma-Aldrich. MCM-41 was carefully chosen so that only the product with an ~4.5 ± 0.25 nm average diameter was purchased. PCN-128 and COF-ETTA-TPDA were synthesized according to the literature[82–84] and confirmed as shown in the Supplemental information (SI; Scheme S1; Figures S1 and S2). Six surface sites of T4L (Figure 2A) were mutated

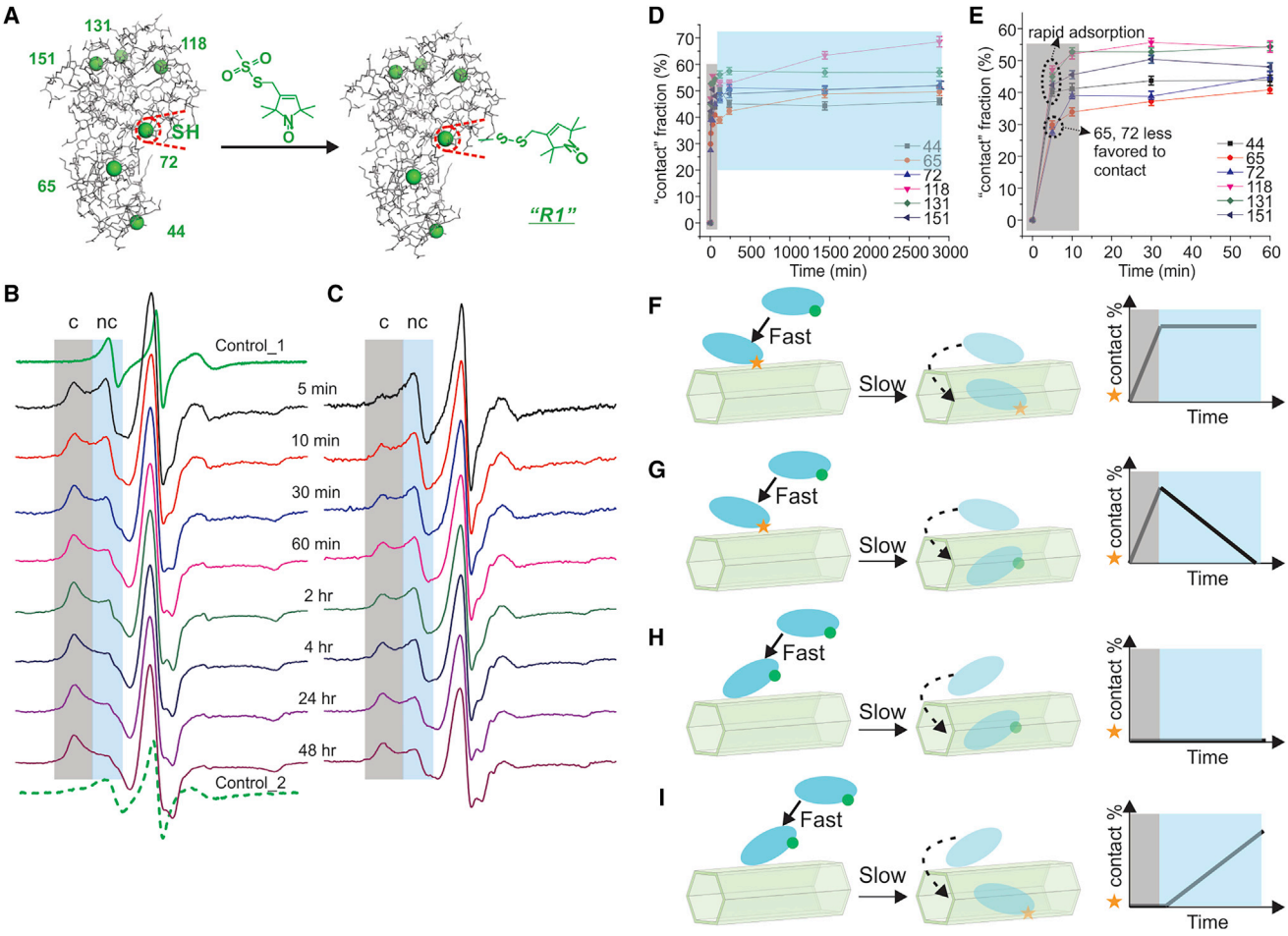

Figure 2. Protein transfer into hydrophobic channels

(A) Six surface sites of T4L selected for probing protein orientation during protein transfer and schematic illustration of protein SDSL. The labeled sites are shown in green spheres, whereas the labeling reagent is in green as well. The cone of a label is highlighted in red. The resultant spin-labeled side chain is designated as "R1."

(B and C) Representative time-resolved CW EPR data on 44R1 and 65R1. Control_1 and Control_2 are free T4L in solution (green trace) and upon immobilization to Sepharose beads (no contact with the labeled sites, green dotted traces). The data at different time points are indicated by the time between (B) and (C).

(D) The relative population of T4L variants that contact the COF-ETTA-TPDA surface over 48 h as determined from spectral simulations. Different labeling sites are color coded. Two major steps of loading kinetics are highlighted in gray and blue shades. Different labeled sites are colored according to the inset. Error bars include the uncertainties over three repeated measurements at each data point and that from spectral simulations.

(E) Amplification of the first 1 h of (D) that highlights the relative preference of different labeled sites to be adsorbed to COF-ETTA-TPDA surfaces. Error bars include the uncertainties over three repeated measurements at each data point and that from spectral simulations. Different labeled sites are colored according to the inset.

(F–I) Four scenarios that describe the relative population of the "contact" fraction changes over time. Green: a label on a protein without contact any surface. Star: the labeled site contacts COF-ETTA-TPDA surface. The real trace of contact percentage over time for each mutant shown in the main text is a combination of any of the four simplified cases.

to cysteines, one at a time, to cover the key regions of T4L surface. Each mutant was then labeled with a methanethiosulfonate nitroxide via a disulfide bond (Figure 2A).[77] After labeling, all six variants were subjected for electrophoresis gel, circular dichroism (CD), and lysozyme activity assay to confirm that the mutation did not alter the molecular weight, secondary structure, and function of the protein (see Supplemental experimental procedures and Figures S3–S5). Also, the continuous wave (CW) EPR spectra of all variants in buffer and upon immobilization to a solid surface were acquired. The resultant spectra shown in Figure S6 were consistent with those

reported in the literature[81,85–87] where the mutation and labeling were confirmed, indicating the success of SDSL to our model protein.

Protein transfer into hydrophobic channels

The principles to determine the relative orientation changes of T4L upon transfer into a channel using time-resolved CW EPR are as follows. CW EPR is sensitive to the local dynamics and therefore contact of T4L-labeled side chain with the channel.[77] Free protein in buffer results in a sharp spectrum due to the fast protein tumbling (Figure 1B, green); upon adsorption to a channel (but the label does not contact channel surfaces) wherein protein rotational tumbling is restricted, a broader spectrum is resolved (Figure 1B, blue). These two cases often result in overlapped spectral components that are designated as the non-contact ("nc") component in this work. When the labeled site contacts the channel, the highly restricted motion leads to a more broadened spectrum that differs from the nc component (designated as the contact ["c"] component; Figure 1B, orange). During protein transfer, all three cases can be present with varied relative populations over time, leading to heterogeneous spectra with multiple components at each time point; spectral analysis based on first principal theories (Figure S7) can deconvolute the relative population of the "c" versus the "nc" spectral components (Figure 1B, right). Therefore, by monitoring the relative population of the two components, it is possible to plot the amount of protein mutants adsorbed by and in contact with a channel (the profile of the "c" component) in real time. Moreover, by revealing the differences among different labeled sites (while confirming that labeling at varied sites does not affect the overall adsorption), the probability of each residue to contact the channel at each loading step will be discovered, leading to protein orientation at each step of a transfer process.

To carry out the time-resolved EPR study, at room temperature, ~0.2 nmol (2 μL, 1 mM) of each labeled T4L mutant was mixed with ~0.2 mg of COF-ETTA-TPDA in 20 μL of HEPES buffer (50 mM, pH 7.2) in an EPR capillary. Next, the spectra were acquired at 16 time points immediately after the mixing (only data at 5 min, 10 min, 30 min, 1 h, 2 h, 4 h, 24 h, and 48 h are shown for conciseness). Representative time-resolved spectra are shown in Figures 2B and 2C (for full dataset, see Figure S8). In each spectrum, two components are resolved (see the low-field region; the "c" and "nc" regions/components are highlighted in gray and blue shades, respectively), with the "c" spectral intensity increased and the "nc" component decreased over time, indicating that the labeled mutant is gradually transferred into the channel.

To quantitatively reveal the loading profile of each variant, spectral simulations were carried out using the established algorithm.[88] The details of the fitting procedure and key parameters are shown in Tables S1–S3, while the quality of simulation is shown by the representative fittings of 44R1 and 65R1 (typical examples of a "rapid" and "slow" initial adsorption, respectively; see below) in Figure S9. The relative percentage of the "c" component for each variant as a function of time is plotted in Figure 2D and amplified in Figure 2E. Overall, a rapid increase in the "c" component is observed within 10–30 min (Figure 2E, gray block), followed by a shallow increase thereafter (Figure 2D, blue block). The two distinct rates of increase in the "c" component can be rationalized into two steps of protein transfer: a rapid protein adsorption to COF-ETTA-TPDA surface and a slow protein entrance into the channels of COF-ETTA-TPDA. The first step is rapid because of the hydrophobic interaction between COF-ETTA-TPDA and T4L, whereas the second step is slow because of the steric hindrance. In particular, all labeled sites except 65 and 72 showed a strong

adsorption (>40% of "c") within 30 min of contact (Figure 2E), indicating strong interactions between these four labeled sites and COF-ETTA-TPDA surfaces. Sites 65 and 72 showed the least preference to adsorb, likely because of the lack of aromatic residues surrounding these two sites (Figure S10A). Next, up to 48 h, a very slow increase in the "c" fraction is observed for all sites, in reasonable agreement with the loading time of enzymes into COF materials.[89] At 48 h, the "c" fraction of each labeled site also indicates that 65R1 and 72R1 have the lowest chance to contact the channels.

From 1 to 48 h (Figure 2D, blue shade), 65, 72, and 118 showed increased "c" fractions, whereas other curves fluctuated or even slightly decreased, indicating a protein site that contacts the channel surface could be detached over time while still being trapped in the channel. Or, the protein inside the channel can change its orientation over time. This finding can be rationalized based on four simplified protein transfer scenarios (Figures 2F–2I). In scenario I, if the labeled site contacts both the surface and the channel of COF (Figure 2F), the "c" component increases upon mixing and remains constant until all proteins enter. In scenario II, if the labeled site only contacts COF surface, but not the channel, after entering the channel (Figure 2G), the "c" component increases upon mixing, but decreases once settled down in the channel. In scenario III, if the labeled site does not contact either the surface or the channel of COF (Figure 2H), the "c" component remains 0. In scenario IV, if the labeled site does not contact the surface, but contacts the channel (Figure 2I), the "c" component remains 0 at the beginning of the transfer, but slowly increases upon entering the channel. In reality, all four scenarios can occur simultaneously; the contribution from each scenario can be different depending on the labeled sites. If scenario II occurs with a high probability, the "c" percentage would decrease over time.

To demonstrate that the observed adsorption is originated from enzyme loading into the channel (but not on the surface) of COF-ETTA-TPDA, two control experiments were carried out. First, the wild-type lysozyme (with no spin label) was "pre-loaded" to saturate COF-ETTA-TPDA (most likely both the surface and the pores of COF-ETTA-TPDA are blocked). Next, a representative site, 65R1, was mixed with this pre-filled COF, followed by immediate monitoring of the EPR signal. The time-resolved EPR data show a constant "nc" component and hardly noticeable "c" peak over time (Figure S11A). This finding suggests no T4L adsorption once the channels and surface of COF-ETTA-TPDA were filled up with a protein. Second, we utilized a large protein, α-amylase, to block the surface of COF-ETTA-TPDA, but not the channel (the amylase is ~54 kDa and much larger in size than the channel diameter), so that T4L can only enter the channels, but there is no surface adsorption. Upon confirming that T4L does not interact with α-amylase (mixture of α-amylase and labeled T4L resulted in the same spectra as Figure S6, left; data not shown). The data shown in Figure S12 confirmed this expectation. Specifically, due to surface blockage, it took about 4 h for the similar amount of 151R1 "c" component (Figure S12B) to raise to the level of the "c" peak at 5 min without surface blockage (Figure S12A). Such a slow increase in the "c" peak indicates that the rapid surface adsorption observed in Figures 2D and 2E disappeared. This is because the surfaces have been saturated by the large amylase and T4L only enters the channels in a much lower rate. These two controls together with our recent studies[49] on protein loading into other COFs unambiguously suggest that the observed change in the "c" EPR component was originated from T4L entering the channel of COF-ETTA-TPDA.

To prove the difference in the loading profiles among different mutants are originated from differences in protein regions that contact the COF surface (but not

caused by R1 side chain and variation in labeling position), we carried out adsorption studies of different spin-labeled mutants using ultraviolet-visible (UV-vis) spectroscopy, which solely detects the amount of free protein in the supernatant, leading to loading profiles. As shown in Figure S13A, the adsorption profiles of two representative mutants, 65R1 and 151R1, are nearly identical to that of the wild-type protein. This suggests that the differences in time-resolved CW EPR spectra are not caused by R1 length or different labeling position. Rather, they are caused by different protein orientation at different stages of the transfer.

We also ruled out the possibility of spin label (radical) degradation by protein desorption or aggregation, which may also cause line shape changes. In doing so, we investigated the spin density of each labeled mutant over time. The double-integrated area of the spectrum at each time point remains near constant through the whole titration process (Figure S14A), suggesting no radical degradation. Note that the "c" peak is unlikely to be originated from protein-protein interactions within the same channel, because such a peak is not present in T4L solutions under very high protein concentrations (data identical to Figure S6, left panel; data not shown).

Taken together, the time-resolved EPR data observed on this COF are originated from protein transfer into the COF channels; the changes in the population of the "c" component are not a result of pure protein adsorption or protein-protein interaction, but the contact of the labeled sites with the channel.

Protein transfer into charged channels

Under neutral pH and room temperature, T4L surface has a positive net charge (isoelectric point [pI] ~ 9.2), while MCM-41 is weakly negatively charged and thus can induce protein transfer driven by electrostatic interactions. To probe this process, ~2 nmol (2 μL, 1 mM) of each labeled T4L was mixed with ~0.2 mg of MCM-41 in 20 μL of HEPES buffer (50 mM, pH 7.2) in an EPR capillary. Next, the time-resolved EPR spectra were acquired at the same time points (for example data, see Figures 3A and 3B; for full dataset, see Figure S15). Similar to the COF-ETTA-TPDA case, over time, the "c" spectral component is increased, while the "nc" component is decreased, indicating the gradual entrance of each variant into the channel. All spectra were then simulated, and the resultant plot of the "c" percentage as a function of time is shown in Figures 3C and 3D for all labeled sites. The quality of fitting is presented in Figure S16 on representative mutants and time points.

Compared with the COF-ETTA-TPDA case, the transfer into MCM-41 shows 3 steps: a rapid increase in the "c" component in the beginning 5–10 min (Figures 3C and 3D, gray shade), a slow increase from 30 min to ~4 h (Figures 3C and 3D, yellow shade), and a much shallower increase/fluctuation until 48 h (Figure 3C). The first step is likely caused by the strong, long-range electrostatic interaction between T4L and MCM-41, which rapidly adsorbs some proteins to the surface (5–10 min). Next, more proteins begin to "stack" on the outer layers (which can increase the "contact" population due to protein-protein "contact"), similar to our recent study;[90] meanwhile, proteins slowly enter the channels during "stacking." Finally, most stacked proteins enter the channel.

Similar to the COF-ETTA-TPDA case, the rate of increase in the "c" fraction in each step is dependent on the labeled sites. From 0 to10 min, 118R1, 44R1, and 131R1 show the most rapid increase in the "c" fraction (Figure 3D, purple triangles, black squares, and green diamonds represent these sites, respectively), likely because these sites are mostly surrounded by positive residues (Figure S10B, top; blue

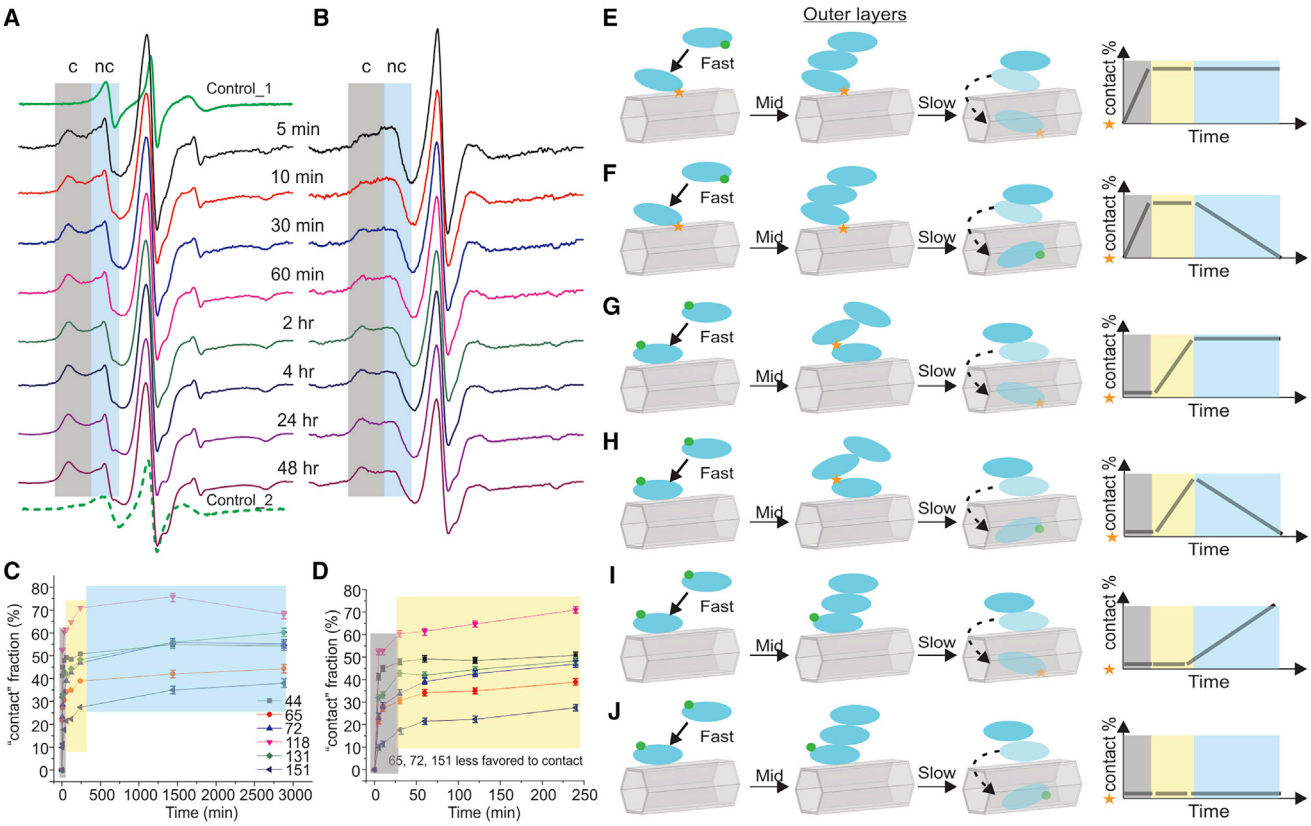

Figure 3. Protein transfer into charged channels

(A and B) Representative time-resolved CW EPR data on 44R1 and 65R1. Control_1 and Control_2 are free T4L in solution (green trace) and upon immobilization to Sepharose beads (green dotted trace).

(C) The relative population of the proteins that contact the MCM-41 surface over 48 h as determined from spectral simulations. Three major steps of loading kinetics are highlighted in gray, yellow, and blue shades, respectively. Different labeled sites are colored according to the inset.

(D) Amplification of the first 4 h of (C) that highlights the relative preference of different labeled sites to be adsorbed to MCM-41 surfaces. Error bars indicate the uncertainties at each data point. Different labeled sites are colored according to the inset.

(E–J) Six scenarios that describe the relative population of the "contact" fraction changes over time. Green: a label on a protein without contact any surface. Star: the labeled site contacts proteins in the outer layers of the multiplex adsorption or MCM-41 surfaces. The real trace of contact percentage over time for each mutant shown in the main text can be a combination of any of the six simplified cases.

represents positive residues) that can strongly interact with the negative MCM-41 surface. 72R1 is surrounded by both positive and negative residues (Figure S10B, bottom) and shows medium increase in the "c" fraction (Figure 3D, blue triangles). 65R1 is mostly surrounded by negative residues (Figure S10B, yellow arrow), whereas 151R1 is likely blocked by steric hindrance (Figure S10B, orange arrow), resulting in the lowest increase in the "c" fraction (Figure 3D, red circles and gray triangles, respectively). From 10 min to 4 h, almost every site shows a similar slope of increase in the "c" fraction (Figure 3D, yellow shade), consistent with random protein orientations during stacking (which resulted in a crowding effect to the involved proteins).[90] From 4 to 48 h, the "c" fraction fluctuates depending on the labeled site, meaning the protein may change its orientation ("c" regions) over time inside of the channel. The "c" fraction of each labeled site at 48 h follows the same trend of the first step, indicating that the final orientation preference also follows 118R1, 44R1, and 131R1 having more chance to contact the channel walls.

The fluctuation or decrease in the "c" fraction in 4–48 h (i.e., Figure 3C, purple) can be understood following six simplified transfer scenarios. Depending on whether the

labeled site contacts the MCM-41 surface, the fraction of the "c" component in the first 10 min can remain 0 or rapidly increase (Figures 3E–3J, gray shades). From 30 min to ~4 h, depending on whether the labeled site contacts on MCM surface or other proteins from the outer layers of the stacking, the fraction of the "c" component can remain 0 or slowly increase (Figures 3E–3J, yellow shades). Last, from 4 to 48 h, depending on whether the labeled mutant contacts the channels of MCM-41 and the status after the second step, the "c" fraction can increase, retain, or decrease (Figures 3E–3J, blue shades). In reality, all six scenarios can occur simultaneously; the contribution from each scenario can be different depending on the labeled sites. If scenarios II or IV occur with a higher population (Figures 3F and 3H), the "c" fraction would decrease over time. We are aware that some scenarios can result in a similar model (that is Figure 2F versus Figure 3E or Figure 2H versus Figure 3J). The key to discriminate these two cases is the number of transition stages/phases/steps: a two-step transition would be consistent with Figure 2F/Figure 2H, whereas a three-step transition indicates the model of Figure 3E/Figure 3J).

To prove the observed adsorption is originated from enzyme loading into the channels (but not the surface) of MCM-41, two control experiments were carried out. First, we saturated the MCM-41 with the unlabeled wild-type T4L before the EPR study (designated as "pre-filled MCM-41"), which should block the surface and the channels of the compartment. Next, a time-resolved CW EPR study was carried out on labeled protein mutants. Our EPR data (Figure S11B) show almost no change in the "c" peak over time, indicating both surface and channels of MCM-41 were blocked. Second, similar to the COF case, we utilized α-amylase to block the surface of MCM-41, but not the channels. The data in Figure S17 show a very slow increase in the "c" peak for the representative site, 151R1, indicating that the rapid surface adsorption (Figures 3C and 3D) is absent. T4L only enters the channels of MCM-41. These controls suggest the three-step adsorption discussed above is originated from enzyme entering the channels of MCM-41.

To rule out the effect of spin label size and rigidity on the loading kinetics, we carried out UV-vis study. As shown in Figure S13B, the adsorption profiles of representative mutants are nearly identical to that of the wild-type protein. This suggests that the differences in time-resolved CW EPR spectra are not caused by R1 length or different labeling position. Also, the differences are not caused by spin label radical degradation over time due to protein desorption or aggregation because the integrated area of the spectrum at each time point remains near identical through the whole titration process (Figure S14B). Thus, the time-resolved EPR data observed on MCM-41 are originated from protein transfer into the MCM-41 channels; the changes in the "c" component are not caused by pure protein adsorption or protein-protein interaction, but by the contact of the labeled sites with the channel.

The "stacking" of proteins on the MCM-41 surface was further supported by transmission electron microscopy (TEM), ξ-potential measurements, attenuated total reflectance Fourier transform infrared spectrometry (ATR-FTIR), and UV absorption. TEM images shown in Figure S19 indicate that upon protein loading, a layer of "cloud" was coated on the surface of MCM-41, which can be removed upon extensive washing. This indicate the presence of proteins stacking out on MCM-41. The surface charge of MCM-41 upon protein mixing rapidly increased (due to the positive net charge of protein), suggesting the protein stacking outside of the channel (but not inside, which would otherwise result in a more negative surface charge; Figure S20). The ATR-FTIR reported the presence of proteins on the surface of MCM-41 as indicated by presence of protein characteristic peaks (Figure S21). Last, the rapid

loading of protein determined by UV suggested the rapid adsorption of protein to MCM-41 (Figure S13B). Because of the steric hindrance of the channels, the rapid adsorption of protein on MCM-41 more likely suggests a stacking process consistent with our recent finding.[83]

Protein transfer into near-neutral channels

At room temperature, ~2 nmol (2 μL, 1 mM) of each labeled T4L was mixed with ~0.2 mg of PCN-128 in 20 μL of HEPES buffer (50 mM, pH 7.2) in an EPR capillary. Time-resolved spectra were acquired at the same time points as before (for representative data, see Figures 4A and 4B). Similar to the two cases above, overtime, the "c" component is increased, while the "nc" component is decreased, indicating the gradual transfer of each variant into the channel.

The spectra were simulated as described above, which also yielded a plot of the "c" component as a function of time (for example data, see Figure 4C). Different from the two cases discussed above, overall, a much slower increase rate of the "c" component was observed for most labeled sites. This can be rationalized to the much weaker interaction between T4L and the PCN-128 channel; the transfer is mostly dependent on the free diffusion of protein in solution. Furthermore, most labeled sites showed similar "protein-channel contact" versus time profiles, indicating that all regions can have comparable chance to contact the PCN-128 channel during transfer (Figure 4C). Or, there is minimal orientation selectivity during such a transfer.

To ensure the observed adsorption is originated from enzyme loading into the channel (but not on the outer surface) of PCN-128, we saturated the surface and channels of PCN-128 with the wild-type lysozyme (no label attached) and monitored the EPR signal over time using a labeled lysozyme mutant. Our time-resolved EPR data show no change over time in both the "c" and "nc" components (for representative data, see Figure S11C). This finding suggests no protein adsorption once PCN-128 was filled up with a small protein. Second, we utilized α-amylase to block the surface of PCN-128. The data were similar to those without such a blockage (close to Figure 4C; data not shown), indicating that blocking the surface does not affect the slow transfer of the protein into this neutral channel. Similar to the MCM-41 case, the UV study of pure adsorption (Figure S13C) and integrated area study (Figure S14C) suggest that the data we observed were caused by protein transfer into the PCN-128 channel with a random orientation.

Complementary data to support the transfer of protein into the channels

To further support our observation of protein transfer into the channels, we have conducted a time-resolved N2 absorption experiment (see Figure S25). As is evident from the data (Table S4), the porous volume of all three channels was gradually reduced upon protein uptake. In addition, we have conducted energy-dispersive X-ray spectroscopy (EDX) (Figure S26), thermogravimetric analysis (TGA) (Figure S27), powder X-ray diffraction (PXRD) (Figure S28), and scanning electron microscopy (SEM) (Figure S29) experiments. The EDX study on protein@COF-ETTA-TPDA indicated the wt % of sulfur increased from 0% (0 min) to 0.18% ± 0.04% at 30 min, 0.36% ± 0.09% at 60 min, and 0.45% ± 0.06% at 1 day. Similarly, EDX on protein@MCM-41 indicated the wt % of sulfur increased from 0% (0 min) to 0.11% ± 0.06% at 30 min, 0.75% ± 0.04% at 60 min, and 1.04% ± 0.13% at 1 day (representative data are shown in Figure S26). These data indicated the gradual entrance of protein into our channels. In addition, TGA data before and after protein loading (Figure S27) clearly demonstrated the entrance of protein into each channel,

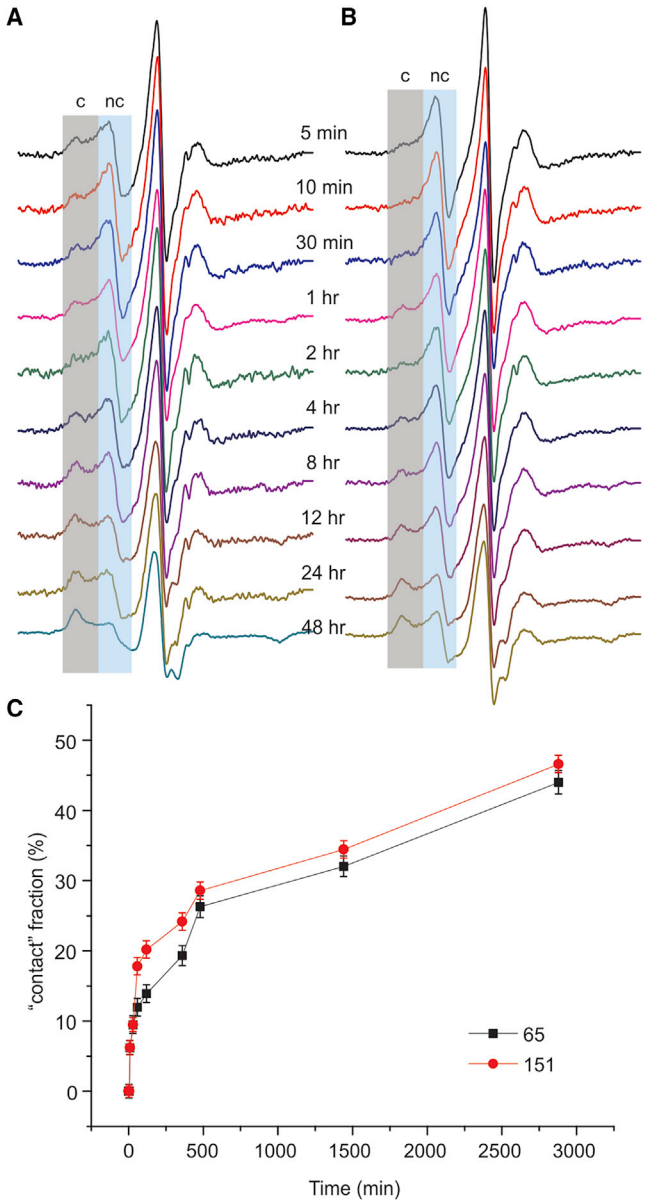

Figure 4. Protein transfer into neutral channels

(A and B) Representative time-resolved CW EPR data on 65R1 and 151R1. EPR data at different time points are indicated by the time between (A) and (B).

(C) The relative population of the representative protein mutants (65, black; 151, red) that contact the PCN-128 surface over 48 h as determined from spectral simulations. Error bars indicate the uncertainties at each data point.

whereas PXRD data (Figure S28) showed that protein loading did not alter the crystallinity of the channels. SEM images (Figure S29) indicate that protein loading did not affect the morphology of the channels.

DISCUSSION

We believe the forces driven the observed protein transfer are related to protein size and surface charge distribution. To evaluate the effect of protein size, we used the

large, rigid protein glucose oxidase (GOx, 80 kDa; ~6.0 × 5.2 × 7.7 nm dimension; in solution, GOx is a dimer, so the actual size is even larger). Although the enzyme in solution is fully active (Figure S22, black), loading the enzyme into the compartments showed no activity but just a baseline (only data from MCM-41 are shown as a representative case of "no activity," indicating no protein transfer into the channels due to the large size of the GOx).

To evaluate the effects of protein surface on the transfer process, we modified our model protein, T4L, with the flexible, near-neutral polymer polyethylene glycol (PEG), due to its softness, which may allow protein entrance to mesopores, as well as its neutral charge, which alters protein surface charge (for full characterization, see our recent work[91]). Our EPR data, shown in Figure S23A, indicate very slow loading of PEG-T4L into PCN-128, suggesting that PEG blocks the protein entrance if only diffusion is the driving force of protein loading. In addition, PEG-T4L is able to enter COF-ETTA-TPDA, as indicated by the increase in the population of the "c" component over time shown in Figure S23B. The rate of loading is much slower than that of free T4L, likely due to the enlarged size. However, due to the presence of hydrophobic interaction, PEG-T4L is able to overcome the size hindrance (also due to the softness of the PEG chain) and enter the channels. Last, we observe very slow entrance of PEG-T4L into MCM-41 (Figure S23C). This indicates that the electrostatic interaction is suppressed, likely by the coating the neutral PEG on protein surface; otherwise, the attractive interactions would pull the protein into the pores, as in the case of COF-ETTA-TPDA.

We also monitored the loading of a negatively charged small protein, lipase. The loading profile was determined via confocal fluorescence imaging. The results (Figure S24) indicated that although it is not impossible for lipase to enter MCM-41, the rate of entrance was much slower than that of the positively charged lysozyme, further confirming the hypothesis that electrostatic interaction is the driving force of lysozyme entrance into MCM-41.

In this work, we selected three channels with different surface charge and hydrophobicity distribution to investigate the overall effects of channel surface properties on and the roles of protein surface charge and hydrophobicity in protein orientation changes during a translocation. We are fully aware that differences in MOF/COF channel charges can also play important roles for T4L transfer, which is indeed the next steps of our ongoing research. The results mentioned above indicate that channel properties have a major impact on the orientation selectivity during protein loading/transfer. For a negatively charged channel, i.e. MCM-41, the strong, long-range, electrostatic interactions rapidly adsorb the protein regions that are surround by positive residues (Figures S10B and S10C), yielding an orientation preference shown in Figure 5A, top panel. Next, a randomly oriented protein stacking occurs (Figure 5A, bottom left panel), followed by the settling down of proteins with a similar orientation preference as in step 1 (Figure 5A, bottom right panel). For a hydrophobic channel, that is COF-ETTA-TPDA, the first step driven by the hydrophobic interactions prefers to orient the protein so that regions with abundant aromatic residues contact the channel surface (Figure 5B, top panel; Figure S10A). Once entered the channel, a similar trend was resolved wherein the protein regions with more aromatic residues more likely contact the walls inside of the channel (Figure 5B, bottom right panel). For a near-neutral channel, that is PCN-128, the diffusion-driven protein transfer occurs with a gradual loading of protein into the channels in long durations. Protein orientation inside of the channel is most likely random (Figure 5C). Overall, our data suggest that protein orientation in each stage of transfer into

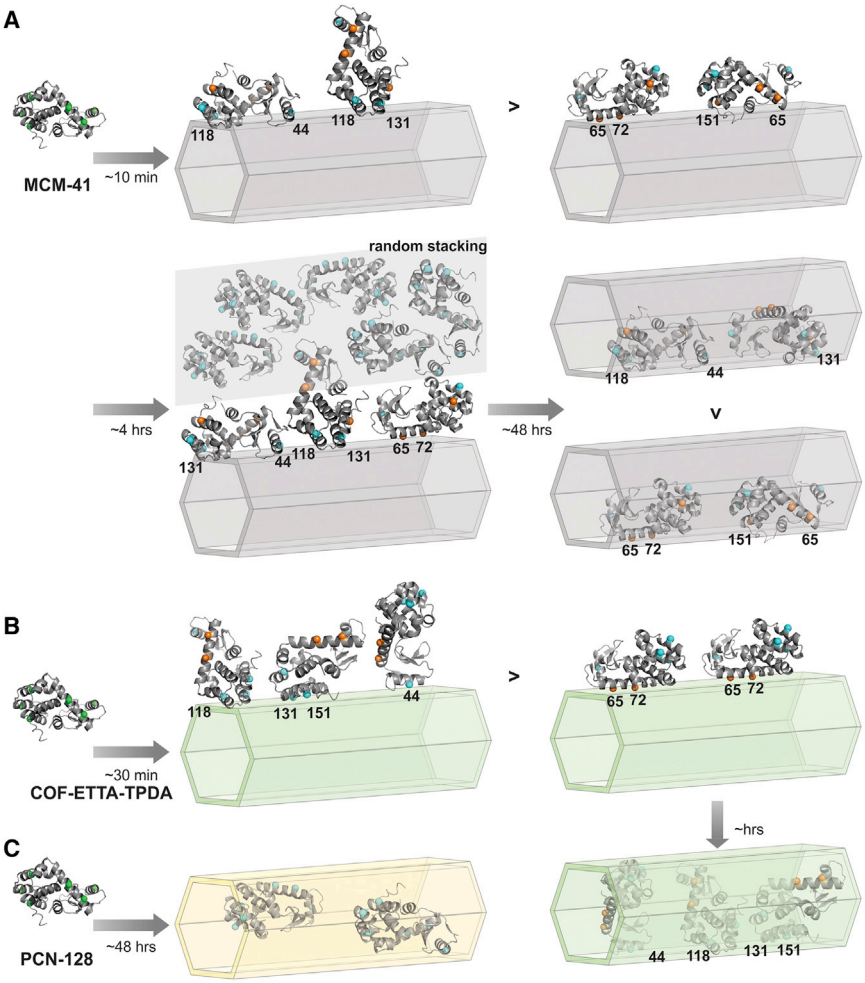

Figure 5. Protein orientations at each step of transfer into different channels

(A–C) The proposed protein transfer mechanisms into a weakly charged (A), hydrophobic (B), and near-neutral (C) channel. The relative orientation of protein at each loading stage is determined based on the preference of each labeled site contacting the surface. The approximate timeline of each step is also shown. Symbol ">" indicates the relative orientation preference.

each channel follows the dominant interactions between the protein and channel. Although the sample volume is relatively low (~20 μL), the gaps among different channels (ca. micrometer scale) are much larger than the size of the protein (2.5 × 3 × 4.5 nm). Thus, the small sample volume is not anticipated to influence the diffusion/transfer of the protein into the channels. Note that due to the small area and the identical chemical composition of the "mouth" of the channels compared with the lateral surfaces, it is impossible to discriminate protein contacts with the mouth from the surfaces. It is possible that proteins adsorbed to the external surface can slide along the surface to enter the channel. However, such sliding most likely does not change the protein orientation with respect to the channel surface and thus, cannot be detected from our EPR technique. Also note that all three particles (Figure S29) are 100–1,000 times larger than the protein (a few nanometers). Therefore, the chance for T4L protein to contact each particle by collision/diffusion is likely similar and, because of this fact, we believe the particle size plays a less important role for the uptake of the smaller protein compared with other properties such as channel surface charge and hydrophobicity.

Because of the complexities caused by the presence of silica, COF, or MOF materials, spectroscopic approaches to probe protein secondary structures such as the CD spectroscopy were not successful in assessing the degree of secondary structural changes during T4L transfer into these channels. Therefore, this situation cannot be excluded. However, substantial lysozyme activity was observed after the protein transfer was completed for all three channels (see Supplemental experimental procedures and Figure S18), suggesting that no major secondary structural changes after the transfer. In addition, the reusability of the loaded protein (Figure S30; see "Lysozyme activity assay" in Supplemental experimental procedures) indicated that the protein was able to retain activity to a certain degree upon transfer into the channels, suggesting that the protein was not seriously damaged during loading. The activity test also indicates that the protein damage upon light irradiation under daylight is negligible. Meanwhile, because CW EPR is sensitive to the local backbone dynamics, or the contact of the labeled site with the channels, our data still determine the relative orientation of T4L on each channel at each probed time point, even if some secondary structural changes occurred during the transfer. In fact, as introduced above, probing the secondary structural changes during a transfer is our ongoing research.

The relative orientation of a model protein, T4L, upon being transferred into nanoscale channels with different surface properties (but a similar diameter) was investigated using SDSL-EPR. It was first confirmed that the observed EPR data are originated from protein transfer into the channels of the three compartments and that the differences in the loading profiles of different labeled protein sites are caused by different ways that the protein contacts the compartment (protein orientation). Depending on the driving force of the protein-channel interaction, the transfer can be viewed as a multi-step process and is dependent on channel properties. For a charged channel, the strong electrostatic interaction with an oppositely charged protein yields a three-step transfer process: (1) protein adsorption to the surface of the channel, (2) protein layers stacking outside of the channel, and (3) protein entering the channel. For a hydrophobic channel, because the hydrophobic interaction is not as strong, the stacking step is less dominant, which resulted in a 2-step transfer process. For a near-neutral channel, a slow loading occurs since diffusion is the primary driving force of loading. Furthermore, based on site-specific backbone dynamics changes of protein reported by time-resolved EPR, the preferential regions of protein that contact the channel at varied time points were revealed, leading to protein orientation preference during each step of the transfer. Thus, dynamic pictured of how T4L is transferred into three representative artificial channels are depicted.

We do not believe lysozyme passes through any of these channels, although certain local translational diffusion may be possible. This is based on the fact that even if we extended the experiment time to 2 weeks, we still did not observe free protein in the sample. This may be caused by the channel lengths of the three studied materials and the steric hindrance of protein diffusion within the channels. Because of the strong protein-channel interactions, to release the loaded proteins, perhaps the best approach would be to unfold the protein to significantly destroy the protein-channel interactions. This experiment, however, is beyond the scope of the investigation in this work. Although the proteins did not pass through the channels, our data will still generate the excitement of developing more sophisticated channels that can better mimic the cellular channels. Toward this goal (which is indeed our ongoing research), we believe that shorter channels close in lengths to the native pores are needed in order to allow proteins to pass through. Furthermore, the

channel properties need to be tuned to be closer to the native channels in terms of size, shape, and hydrophobicity; it will also be useful to align the direction of channels. Last, although challenging, certain functional groups could be included to mimic the selection of native channels against certain proteins. There is clearly a long way to go, so that near-native channels can be developed and channel-based protein translocation processes can be studied in a cell-free platform, which will simplify and speed up the investigation compared with direct in-cell studies.

Our work represents a comprehensive experimental elucidation of protein orientation changes upon transfer into confined, nanoscale, channel-like spaces with different surface properties, which had bridged a long-lasting knowledge gap on protein translocation. The results provide insights into the mechanism of loading proteins into nanoscale compartments, elucidating the translocation or delivery of proteins through cellular protein-conducting channels. Our study is also meaningful for the rational design of synthetic materials as better hosts of enzyme, which improves biocatalysis, and better mimics of the cellular channels so that protein translocation that occurs in the complex cellular environment can be studied in a cell-free platform. The spectroscopic method presented here is applicable to probing the mechanism of protein transfer into other cellular confined spaces such as pockets, cages, and even unstructured shapes, which will broadly impact many essential life processes involving protein translocation.

EXPERIMENTAL PROCEDURES

Resource availability

Lead contact

Further information and requests for resources should be directed to and will be fulfilled by the lead contact, Shengqian Ma (shengqian.ma@unt.edu).

Materials availability

All materials generated in this study are available from the lead contact without restriction.

Data and code availability

The EPR data supporting the current study have not been deposited in a public repository because of the lack of a proper data resource to deposit but are available from the lead contact on request.

Materials and measurements

All chemicals and biochemical supplies were purchased from commercially resources in high purity; the involved experiments were carried out without purification. All characterization, including PXRD, gas adsorption isotherms, SEM, infrared (IR) spectra, and ^{1}H NMR spectra of the involved MOF/COF materials, follows the published procedures using equipment described in our recent work.[49] The expression, purification, and spin labeling of involved lysozyme mutants follow the procedures described in our recent work.[79] For time-resolved EPR measurements, each protein mutant was transferred into a borosilicate capillary tube (0.70 mm inner diameter [i.d.]/1.00 mm outer diameter [o.d.]; Wilmad Labglass) immediately after mixing the channel materials. Data were acquired at varied time points (see main text) using a Varian E-109 spectrometer equipped with a cavity resonator. All CW EPR spectra were obtained with an observe power of 200 mW, a modulation frequency of 100 kHz, and a modulation amplitude of 1.0 G. See Supplemental experimental procedures for full details of synthesis, characterization, and analysis of all materials.

SUPPLEMENTAL INFORMATION

Supplemental information can be found online at https://doi.org/10.1016/j.xcrp.2021.100576.

ACKNOWLEDGMENTS

This work is supported by NSF Career Award (1942596 to Z.Y.). Partial support from NSF (DMR-1352065) and the Welch Foundation (B-0027) is also acknowledged (S.M.). We appreciate Prof. Hubbell for generously providing the EPR spectral simulation package.

AUTHOR CONTRIBUTIONS

Z.Y. and S.M. designed the project. Y.P. and X.W. carried out the experiments and performed the data analysis. H.L., J.R., Y.Z., D.J., I.S., and J.F. assisted in data acquisition and data analysis. H.H. and J.F. assisted in manuscript writing. Z.Y. and S.M. wrote the paper.

DECLARATION OF INTERESTS

The authors declare no competing interests.

Received: May 4, 2021
Revised: July 28, 2021
Accepted: August 24, 2021
Published: September 13, 2021

REFERENCES

1. Firnkes, M., Pedone, D., Knezevic, J., Döblinger, M., and Rant, U. (2010). Electrically facilitated translocations of proteins through silicon nitride nanopores: conjoint and competitive action of diffusion, electrophoresis, and electroosmosis. Nano Lett. *10*, 2162–2167.
2. Niedzwiecki, D.J., Grazul, J., and Movileanu, L. (2010). Single-molecule observation of protein adsorption onto an inorganic surface. J. Am. Chem. Soc. *132*, 10816–10822.
3. Wu, C.-C., Hu, Y., Miller, M., Aroian, R.V., and Sailor, M.J. (2015). Protection and Delivery of Anthelmintic Protein Cry5B to Nematodes Using Mesoporous Silicon Particles. ACS Nano *9*, 6158–6167.
4. Yuan, P., Mao, X., Wu, X., Liew, S.S., Li, L., and Yao, S.Q. (2019). Mitochondria-Targeting. Angew. Chem. Int. Ed. Engl. *58*, 7657–7661.
5. Küchler, A., Yoshimoto, M., Luginbühl, S., Mavelli, F., and Walde, P. (2016). Enzymatic reactions in confined environments. Nat. Nanotechnol. *11*, 409–420.
6. Zhou, H.-X., Rivas, G., and Minton, A.P. (2008). Macromolecular crowding and confinement: biochemical, biophysical, and potential physiological consequences. Annu. Rev. Biophys. *37*, 375–397.
7. Pfanner, N., and Geissler, A. (2001). Versatility of the mitochondrial protein import machinery. Nat. Rev. Mol. Cell Biol. *2*, 339–349.
8. Pfanner, N., Warscheid, B., and Wiedemann, N. (2019). Mitochondrial proteins: from biogenesis to functional networks. Nat. Rev. Mol. Cell Biol. *20*, 267–284.
9. Dolezal, P., Likic, V., Tachezy, J., and Lithgow, T. (2006). Evolution of the molecular machines for protein import into mitochondria. Science *313*, 314–318.
10. Soll, J., and Schleiff, E. (2004). Protein import into chloroplasts. Nat. Rev. Mol. Cell Biol. *5*, 198–208.
11. Ellgaard, L., and Helenius, A. (2003). Quality control in the endoplasmic reticulum. Nat. Rev. Mol. Cell Biol. *4*, 181–191.
12. Tsai, B., Ye, Y., and Rapoport, T.A. (2002). Retro-translocation of proteins from the endoplasmic reticulum into the cytosol. Nat. Rev. Mol. Cell Biol. *3*, 246–255.
13. Liu, J., Peng, J., Shen, S., Jin, Q., Li, C., and Yang, Q. (2013). Enzyme entrapped in polymer-modified nanopores: the effects of macromolecular crowding and surface hydrophobicity. Chemistry *19*, 2711–2719.
14. Mittal, J., and Best, R.B. (2008). Thermodynamics and kinetics of protein folding under confinement. Proc. Natl. Acad. Sci. USA *105*, 20233–20238.
15. Kim, Y.E., Hipp, M.S., Bracher, A., Hayer-Hartl, M., and Hartl, F.U. (2013). Molecular chaperone functions in protein folding and proteostasis. Annu. Rev. Biochem. *82*, 323–355.
16. Finka, A., Mattoo, R.U.H., and Goloubinoff, P. (2016). Experimental Milestones in the Discovery of Molecular Chaperones as Polypeptide Unfolding Enzymes. Annu. Rev. Biochem. *85*, 715–742.
17. Rapoport, T.A., Li, L., and Park, E. (2017). Structural and Mechanistic Insights into Protein Translocation. Annu. Rev. Cell Dev. Biol. *33*, 369–390.
18. Bonardi, F., Nouwen, N., Feringa, B.L., and Driessen, A.J.M. (2012). Protein conducting channels-mechanisms, structures and applications. Mol. Biosyst. *8*, 709–719.
19. Simon, S.M. (1995). Protein-conducting channels for the translocation of proteins into and across membranes. Cold Spring Harb. Symp. Quant. Biol. *60*, 57–69.
20. Wickner, W., and Schekman, R. (2005). Protein translocation across biological membranes. Science *310*, 1452–1456.
21. Rapoport, T.A. (2007). Protein translocation across the eukaryotic endoplasmic reticulum and bacterial plasma membranes. Nature *450*, 663–669.
22. Hansen, K.G., and Herrmann, J.M. (2019). Transport of Proteins into Mitochondria. Protein J. *38*, 330–342.
23. Neupert, W., and Herrmann, J.M. (2007). Translocation of proteins into mitochondria. Annu. Rev. Biochem. *76*, 723–749.
24. Marom, M., Azem, A., and Mokranjac, D. (2011). Understanding the molecular mechanism of protein translocation across the mitochondrial inner membrane: still a long way to go. Biochim. Biophys. Acta *1808*, 990–1001.

25. Braakman, I., and Bulleid, N.J. (2011). Protein folding and modification in the mammalian endoplasmic reticulum. Annu. Rev. Biochem. *80*, 71–99.

26. Lee, M.C.S., Miller, E.A., Goldberg, J., Orci, L., and Schekman, R. (2004). Bi-directional protein transport between the ER and Golgi. Annu. Rev. Cell Dev. Biol. *20*, 87–123.

27. Zimmermann, R., Eyrisch, S., Ahmad, M., and Helms, V. (2011). Protein translocation across the ER membrane. Biochim. Biophys. Acta *1808*, 912–924.

28. Guo, Y., Sirkis, D.W., and Schekman, R. (2014). Protein sorting at the trans-Golgi network. Annu. Rev. Cell Dev. Biol. *30*, 169–206.

29. Teasdale, R.D., and Jackson, M.R. (1996). Signal-mediated sorting of membrane proteins between the endoplasmic reticulum and the golgi apparatus. Annu. Rev. Cell Dev. Biol. *12*, 27–54.

30. Glick, B.S., and Nakano, A. (2009). Membrane traffic within the Golgi apparatus. Annu. Rev. Cell Dev. Biol. *25*, 113–132.

31. Li, H.M., and Chiu, C.-C. (2010). Protein transport into chloroplasts. Annu. Rev. Plant Biol. *61*, 157–180.

32. Schleiff, E., and Becker, T. (2011). Common ground for protein translocation: access control for mitochondria and chloroplasts. Nat. Rev. Mol. Cell Biol. *12*, 48–59.

33. Jarvis, P., and López-Juez, E. (2013). Biogenesis and homeostasis of chloroplasts and other plastids. Nat. Rev. Mol. Cell Biol. *14*, 787–802.

34. Keegstra, K. (1989). Transport and routing of proteins into chloroplasts. Cell *56*, 247–253.

35. Subramani, S., Koller, A., and Snyder, W.B. (2000). Import of peroxisomal matrix and membrane proteins. Annu. Rev. Biochem. *69*, 399–418.

36. Plemper, R.K., and Wolf, D.H. (1999). Retrograde protein translocation: ERADication of secretory proteins in health and disease. Trends Biochem. Sci. *24*, 266–270.

37. Wang, M., and Kaufman, R.J. (2016). Protein misfolding in the endoplasmic reticulum as a conduit to human disease. Nature *529*, 326–335.

38. Kang, Y., Fielden, L.F., and Stojanovski, D. (2018). Mitochondrial protein transport in health and disease. Semin. Cell Dev. Biol. *76*, 142–153.

39. Zimmermann, R., Müller, L., and Wullich, B. (2006). Protein transport into the endoplasmic reticulum: mechanisms and pathologies. Trends Mol. Med. *12*, 567–573.

40. Bexiga, M.G., and Simpson, J.C. (2013). Human diseases associated with form and function of the Golgi complex. Int. J. Mol. Sci. *14*, 18670–18681.

41. Chaudhuri, T.K., and Paul, S. (2006). Protein-misfolding diseases and chaperone-based therapeutic approaches. FEBS J. *273*, 1331–1349.

42. Ebrahimi-Fakhari, D., Saidi, L.-J., and Wahlster, L. (2013). Molecular chaperones and protein folding as therapeutic targets in Parkinson's disease and other synucleinopathies. Acta Neuropathol. Commun. *1*, 79.

43. Bayne, L., Ulijn, R.V., and Halling, P.J. (2013). Effect of pore size on the performance of immobilised enzymes. Chem. Soc. Rev. *42*, 9000–9010.

44. Lian, X., Fang, Y., Joseph, E., Wang, Q., Li, J., Banerjee, S., Lollar, C., Wang, X., and Zhou, H.-C. (2017). Enzyme-MOF (metal-organic framework) composites. Chem. Soc. Rev. *46*, 3386–3401.

45. Drout, R.J., Robison, L., and Farha, O.K. (2019). Catalytic applications of enzymes encapsulated in metal-organic frameworks. Coord. Chem. Rev. *381*, 151–160.

46. Schnell, D.J., and Hebert, D.N. (2003). Protein translocons: multifunctional mediators of protein translocation across membranes. Cell *112*, 491–505.

47. Pfanner, N., and Chacinska, A. (2002). The mitochondrial import machinery: preprotein-conducting channels with binding sites for presequences. Biochim. Biophys. Acta *1592*, 15–24.

48. Tai, J., Dave, K., Hahn, V., Guzman, I., and Gruebele, M. (2016). Subcellular modulation of protein VlsE stability and folding kinetics. FEBS Lett. *590*, 1409–1416.

49. Sun, Q., Pan, Y., Wang, X., Li, H., Farmakes, J., Aguila, B., Yang, Z., and Ma, S. (2019). Mapping out the Degree of Freedom of Hosted Enzymes in Confined Spatial Environments. Chem *5*, 3184–3195.

50. Ma, X., and Zhao, Y. (2015). Biomedical Applications of Supramolecular Systems Based on Host-Guest Interactions. Chem. Rev. *115*, 7794–7839.

51. Chen, B., Xiang, S., and Qian, G. (2010). Metal-organic frameworks with functional pores for recognition of small molecules. Acc. Chem. Res. *43*, 1115–1124.

52. Cooke, G., and Rotello, V.M. (2002). Methods of modulating hydrogen bonded interactions in synthetic host-guest systems. Chem. Soc. Rev. *31*, 275–286.

53. Dong, Z., Sun, Y., Chu, J., Zhang, X., and Deng, H. (2017). Multivariate Metal-Organic Frameworks for Dialing-in the Binding and Programming the Release of Drug Molecules. J. Am. Chem. Soc. *139*, 14209–14216.

54. Houk, K.N., Leach, A.G., Kim, S.P., and Zhang, X. (2003). Binding affinities of host-guest, protein-ligand, and protein-transition-state complexes. Angew. Chem. Int. Ed. Engl. *42*, 4872–4897.

55. Hanefeld, U., Gardossi, L., and Magner, E. (2009). Understanding enzyme immobilisation. Chem. Soc. Rev. *38*, 453–468.

56. Sakakibara, D., Sasaki, A., Ikeya, T., Hamatsu, J., Hanashima, T., Mishima, M., Yoshimasu, M., Hayashi, N., Mikawa, T., Wälchli, M., et al. (2009). Protein structure determination in living cells by in-cell NMR spectroscopy. Nature *458*, 102–105.

57. Theillet, F.-X., Binolfi, A., Bekei, B., Martorana, A., Rose, H.M., Stuiver, M., Verzini, S., Lorenz, D., van Rossum, M., Goldfarb, D., and Selenko, P. (2016). Structural disorder of monomeric α-synuclein persists in mammalian cells. Nature *530*, 45–50.

58. Spruijt, E., Sokolova, E., and Huck, W.T.S. (2014). Complexity of molecular crowding in cell-free enzymatic reaction networks. Nat. Nanotechnol. *9*, 406–407.

59. Liu, A.P., and Fletcher, D.A. (2009). Biology under construction: in vitro reconstitution of cellular function. Nat. Rev. Mol. Cell Biol. *10*, 644–650.

60. Talaga, D.S., and Li, J. (2009). Single-molecule protein unfolding in solid state nanopores. J. Am. Chem. Soc. *131*, 9287–9297.

61. Li, H., Pan, Y., Farmakes, J., Xiao, F., Liu, G., Chen, B., Zhu, X., Rao, J., and Yang, Z. (2019). A sulfonated mesoporous silica nanoparticle for enzyme protection against denaturants and controlled release under reducing conditions. J. Colloid Interface Sci. *556*, 292–300.

62. Díaz, J.F., and Balkus, K.J. (1996). Enzyme immobilization in MCM-41 molecular sieve. J. Mol. Catal. B Enzym. *2*, 115–126.

63. Hudson, S., Cooney, J., and Magner, E. (2008). Proteins in mesoporous silicates. Angew. Chem. Int. Ed. Engl. *47*, 8582–8594.

64. Magner, E. (2013). Immobilisation of enzymes on mesoporous silicate materials. Chem. Soc. Rev. *42*, 6213–6222.

65. Lee, C.-H., Lin, T.-S., and Mou, C.-Y. (2009). Mesoporous materials for encapsulating enzymes. Nano Today *4*, 165–179.

66. Zhou, Z., and Hartmann, M. (2013). Progress in enzyme immobilization in ordered mesoporous materials and related applications. Chem. Soc. Rev. *42*, 3894–3912.

67. Howarth, A.J., Liu, Y., Li, P., Li, Z., Wang, T.C., Hupp, J.T., and Farha, O.K. (2016). Chemical, thermal and mechanical stabilities of metal-organic frameworks. Nat. Rev. Mater. *1*, 15018.

68. Majewski, M.B., Howarth, A.J., Li, P., Wasielewski, M.R., Hupp, J.T., and Farha, O.K. (2017). Enzyme encapsulation in metal-organic frameworks for applications in catalysis. CrystEngComm *19*, 4082–4091.

69. Li, P., Modica, J.A., Howarth, A.J., Vargas, L.E., Moghadam, P.Z., Snurr, R.Q., Mrksich, M., Hupp, J.T., and Farha, O.K. (2016). Toward Design Rules for Enzyme Immobilization in Hierarchical Mesoporous Metal-Organic Frameworks. Chem *1*, 154–169.

70. Doonan, C., Riccò, R., Liang, K., Bradshaw, D., and Falcaro, P. (2017). Metal-Organic Frameworks at the Biointerface: Synthetic Strategies and Applications. Acc. Chem. Res. *50*, 1423–1432.

71. Gkaniatsou, E., Sicard, C.m., Ricoux, R.m., Mahy, J.-P., Steunou, N., and Serre, C. (2017). Metal-organic frameworks: a novel host platform for enzymatic catalysis and detection. Mater. Horiz. *4*, 55–63.

72. Deng, H., Grunder, S., Cordova, K.E., Valente, C., Furukawa, H., Hmadeh, M., Gándara, F., Whalley, A.C., Liu, Z., Asahina, S., et al. (2012). Large-pore apertures in a series of metal-organic frameworks. Science *336*, 1018–1023.

73. Wälti, M.A., Libich, D.S., and Clore, G.M. (2018). Extensive Sampling of the Cavity of the GroEL Nanomachine by Protein Substrates Probed by Paramagnetic Relaxation Enhancement. J. Phys. Chem. Lett. *9*, 3368–3371.

74. Libich, D.S., Tugarinov, V., Ghirlando, R., and Clore, G.M. (2017). Confinement and Stabilization of Fyn SH3 Folding Intermediate Mimetics within the Cavity of the Chaperonin GroEL Demonstrated by Relaxation-Based NMR. Biochemistry *56*, 903–906.

75. Fawzi, N.L., Ying, J., Ghirlando, R., Torchia, D.A., and Clore, G.M. (2011). Atomic-resolution dynamics on the surface of amyloid-β protofibrils probed by solution NMR. Nature *480*, 268–272.

76. Wälti, M.A., Schmidt, T., Murray, D.T., Wang, H., Hinshaw, J.E., and Clore, G.M. (2017). Chaperonin GroEL accelerates protofibril formation and decorates fibrils of the Het-s prion protein. Proc. Natl. Acad. Sci. USA *114*, 9104–9109.

77. Hubbell, W.L., López, C.J., Altenbach, C., and Yang, Z. (2013). Technological advances in site-directed spin labeling of proteins. Curr. Opin. Struct. Biol. *23*, 725–733.

78. Hubbell, W.L., Cafiso, D.S., and Altenbach, C. (2000). Identifying conformational changes with site-directed spin labeling. Nat. Struct. Biol. *7*, 735–739.

79. Pan, Y., Li, H., Farmakes, J., Xiao, F., Chen, B., Ma, S., and Yang, Z. (2018). How Do Enzymes Orient When Trapped on Metal-Organic Framework (MOF) Surfaces? J. Am. Chem. Soc. *140*, 16032–16036.

80. López, C.J., Fleissner, M.R., Brooks, E.K., and Hubbell, W.L. (2014). Stationary-phase EPR for exploring protein structure, conformation, and dynamics in spin-labeled proteins. Biochemistry *53*, 7067–7075.

81. López, C.J., Fleissner, M.R., Guo, Z., Kusnetzow, A.K., and Hubbell, W.L. (2009). Osmolyte perturbation reveals conformational equilibria in spin-labeled proteins. Protein Sci. *18*, 1637–1652.

82. Ascherl, L., Sick, T., Margraf, J.T., Lapidus, S.H., Calik, M., Hettstedt, C., Karaghiosoff, K., Döblinger, M., Clark, T., Chapman, K.W., et al. (2016). Molecular Docking Sites Designed for the Generation of Highly Crystalline Covalent Organic Frameworks. Nat. Chem. *8*, 310–316.

83. Li, P., Chen, Q., Wang, T.C., Vermeulen, N.A., Mehdi, B.L., Dohnalkova, A., Browning, N.D., Shen, D., Anderson, R., Gómez-Gualdrón, D.A., et al. (2018). Hierarchically Engineered Mesoporous Metal-Organic Frameworks toward Cell-free Immobilized Enzyme Systems. Chem *4*, 1022–1034.

84. Li, P., Moon, S.-Y., Guelta, M.A., Harvey, S.P., Hupp, J.T., and Farha, O.K. (2016). Encapsulation of a Nerve Agent Detoxifying Enzyme by a Mesoporous Zirconium Metal-Organic Framework Engenders Thermal and Long-Term Stability. J. Am. Chem. Soc. *138*, 8052–8055.

85. Columbus, L., Kálai, T., Jekö, J., Hideg, K., and Hubbell, W.L. (2001). Molecular motion of spin labeled side chains in α-helices: analysis by variation of side chain structure. Biochemistry *40*, 3828–3846.

86. Kroncke, B.M., Horanyi, P.S., and Columbus, L. (2010). Structural origins of nitroxide side chain dynamics on membrane protein α-helical sites. Biochemistry *49*, 10045–10060.

87. Fleissner, M.R., Cascio, D., and Hubbell, W.L. (2009). Structural origin of weakly ordered nitroxide motion in spin-labeled proteins. Protein Sci. *18*, 893–908.

88. Budil, D.E., Lee, S., Saxena, S., and Freed, J.H. (1996). Nonlinear-Least-Squares Analysis of Slow-Motion EPR Spectra in One and Two Dimensions Using a Modified Levenberg-Marquardt Algorithm. J. Magn. Reson. A *120*, 155–189.

89. Sun, Q., Fu, C.-W., Aguila, B., Perman, J., Wang, S., Huang, H.-Y., Xiao, F.-S., and Ma, S. (2018). Pore Environment Control and Enhanced Performance of Enzymes Infiltrated in Covalent Organic Frameworks. J. Am. Chem. Soc. *140*, 984–992.

90. Pan, Y., Neupane, S., Farmakes, J., Bridges, M., Froberg, J., Rao, J., Qian, S.Y., Liu, G., Choi, Y., and Yang, Z. (2017). Probing the structural basis and adsorption mechanism of an enzyme on nano-sized protein carriers. Nanoscale *9*, 3512–3523.

91. Pan, Y., Neupane, S., Farmakes, J., Oh, M., Bentz, K., Choi, Y., and Yang, Z. (2018). Insights on the Structure, Molecular Weight and Activity of an Antibacterial Protein-Polymer Hybrid. ChemPhysChem *19*, 651–658.